Solvent Impact on Langmuir and Langmuir–Schaefer Films of Soluble Main-Chain Poly(fullerene)s Based on C60

Lucas Vinicius de Lima Citolino, Hugo Santos Silva, Deuber Lincon Silva Agostini, Roger Clive Hiorns, Didier Bégué, Clarissa de Almeida Olivati

Solvent impact on Langmuir and Langmuir-Schaefer films of soluble main-chain poly(fullerene)s based on C_{60}

Lucas Vinicius de Lima Citolino*, Hugo Santos Silva, Deuber Lincon Silva Agostini, Roger C. Hiorns, Didier Bégué Clarissa de Almeida Olivati

L. V. L. Citolino, D. L. S. Agostini, C. A. Olivati
School of Science and Technology, São Paulo State University
Physics Department
Presidente Prudente, CP 467, 19060-900, Brazil
E-mail: lucas.citolino@unesp.br

L. V. L. Citolino, H. S. Silva, R. C. Hiorns, D. Bégué

Université de Pau et des Pays de L'Adour, E2S UPPA, CNRS, IPREM, Institut des Sciences Analytiques et de Physico-chimie pour L'Environnement et Les Materiaux, 64000 Pau, France

Keywords: Poly(fullerene)s, thin films, Langmuir-Schaefer, structure-optoelectronic property relationships

Abstract

Understanding the morphology and electronic properties of poly(fullerene)s is crucial for the development of new organic devices. This work addresses the fabrication and characterization of Langmuir–Schaefer (LS) films of poly(fullerene)s based on C_{60} with short (HSS8) and long (HSS16) sidechains, solubilized in chloroform or xylene. In addition, density functional theory (DFT) calculations are used to optimize the molecular geometries, determine energies, and investigate the influence of solvent applied. Depending on the organic solvent, floating material isotherms indicate the formation of disordered aggregates in the aqueous subphase. The influence of solvent in LS films is also evidenced by way of atomic force microscopy (AFM), UV-vis, and cyclic voltammetry (CV) measurements. From DFT calculations, the arms of the poly(fullerene)s start to extend from an initial position of surrounding the fullerene sphere. In AFM measurements, depending on the organic solvent, the roughness significantly reduces, while the homogeneity is much higher. In UV-vis and CV measurements, the propensity to form aggregates depends mainly on the polarization of the solvent and is directly related to the maximum absorption, oxidation, and reduction peaks. From the optical bandgap energy values, the poly(fullerene)s studied here present high potential for application in organic electronic devices.

1. Introduction

Population growth and global economic activities are resulting in an increasing expansion in the production, distribution and consumption of energy, which leads to increased efforts in scientific studies to develop alternatives to fossil fuels to reduce their impacts on the environment.[1,2] Thus, the development of organic photovoltaics (OPVs) constitutes an important study and a vast potential for application, since solar energy is the only inexhaustible source of energy on Earth.[3] In this sense, a thorough investigation of new organic materials is imperative, since the efforts continue in the search and development of low-cost solar cells with economic potential.[4,5]

OPVs based on the so-called bulk-heterojunction (BHJ) active layer have been the most successful of organic devices. The BHJ is a blend of electron donor and electron acceptor materials are intimately mixed so that once light creates an excited state in either of them, a formation of charges at their interface can be rapidly carried out. Efficiencies have so far reached around 19%.[6] In particular, tertiary devices, showing improved stabilities and exceptionally wide absorption profiles, have been particularly successful. They contain both fullerene and non-fullerene acceptors (NFAs) in the BHJ along with a single donor polymer.[7,8] The optical absorption of the fullerene is complementary to that of the polymer and NFA, in addition to bringing higher stability to the devices when exposed to the environment.[7,8] It should be noted that fullerene derivatives by themselves, while widely used in OPVs due to their high electron affinity, in addition to the absorbances constrained to the UV- blue regions, do have low solubilities and poor stabilities due to their tendency to aggregate.[9,10]

In this context, poly(fullerene)s have been proposed in the role of n-type material in all-polymer blends and as electron-selective-layer in devices.[11,12] In particular, main-chain poly(fullerene)s, where the fullerene resides in the polymer backbone, can be obtained through facile syntheses, and present a modular structure which is relatively easy to change. [11,12] The novel solid-state behavior of main-chain poly(fullerene)s make them promising materials for photovoltaic applications.[11,12] In a study by Todor-Boer *et al*. shows that poly(fullerene) systems can exhibit strong photoluminescence quenching with a variety of conjugated electron donor polymers, leading to higher exciton separation at the donor–acceptor interfaces, playing a crucial role in OPV performances.[]

Among the techniques used to fabricate thin-films, the Langmuir, Langmuir-Blodgett (LB) and Langmuir-Schaefer (LS) techniques stand out, as they provide higher organization at the molecular level and control over the thickness and uniformity of the thin film.[13,14] Thus, Langmuir techniques and poly(fullerene)s make an interesting combination, since under well-

defined experimental conditions, it is possible to characterize the organization of the archetypal fullerene derivative [6,6]-phenyl-C_{61}-butyric acid methyl ester (PCBM) and poly(fullerene)s as monolayers due to their hydrophobic properties.[15]

Herein, Langmuir and LS films were fabricated from solutions of the pristine main-chain poly(fullerene)s shown in Figure 1, namely, HSS8 with short -OC_8H_{17} sidechains and HSS16 with long -$OC_{16}H_{33}$ sidechains, to investigate their self-assembly and aggregation with respect to the organic solvent used. Atomic force microscopy (AFM) was performed to inspect the influence of chloroform or xylene on the surface of the solid film features. UV-Visible and cyclic voltammetry (CV) measurements were carried out to examine the absorption, oxidation and reduction peaks that are of direct relevance to organic electronic devices performance. In addition, density functional theory (DFT) calculations were used to optimize the molecular geometries and determine energies, and investigate how the side chains influence if different solvent applied in view of polarity and dipole moment and their solvation structure.[16] Thus, the outcome from all performed characterizations furnished tools to further evaluate the relationships between supramolecular arrangement and optoelectronic properties.

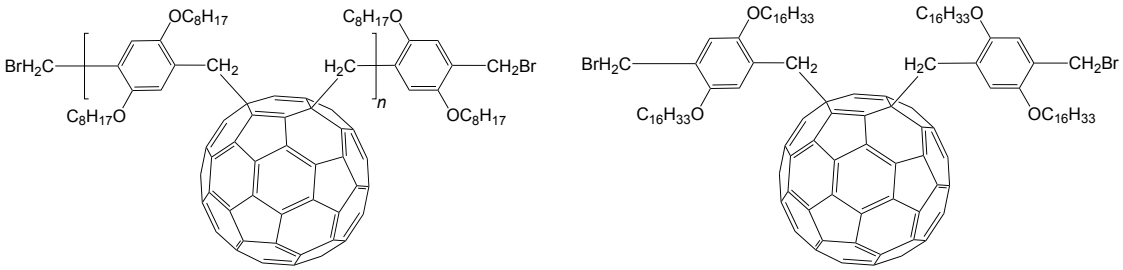

Figure 1. Structures of the two polymers used in this study (left) HSS8 and (right) HSS16.

2. Results and Discussion

2.1. Langmuir films and DFT

The Langmuir technique stands out among the others because it provides higher organization at the molecular level and control over the thickness and uniformity of thin films, thus becoming an important tool for studying the organization of poly(fullerene)s spread as very thin layers at the water-air interface. Figure 1 shows the surface pressure versus the mean area isotherms (π–A) of HSS8 and HSS16, both of them previously solubilized in either chloroform or xylene (0.2 mg/mL).

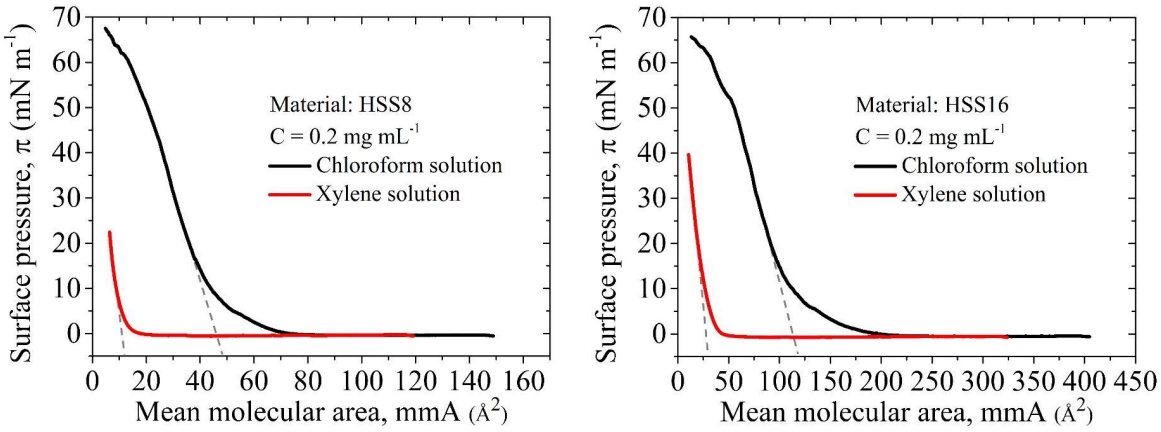

Figure 1. π–A isotherms of HSS8 (to the left) and HSS16 (to the right).

As the materials are closely related to PCBM, it is compelling to start with the interpretation of PCBM isotherms because it is possible to find many literature reports regarding fullerene-type monolayers.[15, 16] According to the literature, in PCBM isotherms, it is possible notice the absence of the usual sharp phase transitions of the typical molecule isotherms, and this is a strong indication that this is a liquid-expanded isotherm (according to Harkins' classification), so, the isotherms show a strong indication of the formation of disordered aggregates onto the aqueous subphase.[15, 15+1, 16+1] The cross-surface area of PCBM is 100 Å^2 and the estimated area from the π–A isotherms range from 9.0 to 30 Å^2; this means that there is a strong aggregation of PCBM regardless of the solvent used.[15, 16]

These results may be due the functional group of the molecule generally being oriented towards the water, a vertical build-up of the molecules in the air–water interface, and this can be a major contribution for the area, and therefore the apparent values are reduced. [15, 16] As reported by Roncaselli *et al.*, the mean area for the PCBM is 23 and 9 Å^2 when in chloroform and xylene solutions, respectively, suggesting that water surfaces are less appealing to the PCBM when coming from these solutions. [15] Surprisingly, even when in good non-polar solvents such as xylene, one cannot ignore the possibility that PCBM readily forms very small nanoaggregates of several units that arises from the strong fullerene-fullerene interactions, hindering the formation of a true monolayer. [15]

In Figure 1, it is possible to see the pristine poly(fullerene)s with isotherms obtained at the Langmuir trough. The area per monomer found for HSS8 was 48 and 12 Å^2 for chloroform and xylene solution, respectively, while, for HSS16 was 126 and 33 Å^2 for chloroform and xylene solution, respectively. In regard to the isotherms, it can be observed that the polymers, like the PCBM, can be classified as a liquid-expanded type, not achieving the phase related to a condensed phase either.[15, 16] However, the overall isotherm behaviors are quite divergent

from one another. The HSS8, both chloroform and xylene solution, present no distinct phase transitions and has a rather steady upward trend until it reaches the collapse pressure. The collapse pressure for chloroform is 62 mN/m, while, for xylene, the isotherm does not reach the collapse pressure. With HSS16, we find that the collapse pressure for chloroform is 52 mN/m, and, again, for xylene, the isotherm does not reach a collapse pressure. A possible explanation is that the arrangement and interaction of these materials on the aqueous surface change according to the functional group of each material, which is generally water-oriented, explaining the differences between the areas obtained in the analysis of isotherms, with HSS16 showing the largest area and HSS8 showing the intermediate area in relation to the area of the PCBM.[15, 16]

A relationship can be established between the solvent used and the molecular area obtained in the study of isotherms by using the data shown in Table 1. The use of different solvents changes the arrangement of molecules because these materials have a low solubility in chloroform, so we found a relatively larger area, while for the xylene solvent, these areas decreased considerably, suggesting that the water surfaces is less appealing to the poly(fullerene) when coming from these solutions, indicating a higher degree of solvation and a lower level of aggregation. [15]

Table 1. Area per molecule for different types of poly(fullerene) solutions

Solution	Area per molecule [Å^2]		
	PCBM	HSS8	HSS16
chloroform	23 [2]	48	126
xylene	9 [2]	12	33

Since there is no previous literature from these exact polymers, to estimate monomer areas, were carried out the theoretical calculations using DFT/B3LYP/6-31+G(d) method for optimizations of geometries and energies. Calculations were performed using the Gaussian 09 program package. DFT calculations were combined with the Grimme's D3 method to account for longer range dispersion interactions.

According to the DFT/6-31+G(d) results presented in Figure 2, HSS8 and HSS16 have structural differences. HSS16 has an elongation (i) in the ‘X’ direction of about 34% compared

to HSS8; (ii) in the 'Y' direction, has an elongation direction of about 19% compared to HSS8; and (iii) in the 'Z' direction, HSS8 has a shortening of about 6%. Table 2 presents the areas of the monomers calculated based on the DFT results. To avoid 'crossing' each other, the arms of the HSS16 molecules (although surrounding mostly the fullerene) start to extend. We found that the calculated molecular areas are all higher than the ones estimated in the π–A isotherms of Figure 1 and Table 1, indicating that both materials aggregate in the Langmuir trough. In spite of this, the areas obtained by DFT are smaller in 'XY' and 'XZ' planes than that in the 'YZ' plane, which suggests an orientation closer to a 'XY' or 'XZ' configuration against the air–water interface. Another important point is the volume occupied by these materials; HSS8 is 42% smaller than HSS16, which is a significant difference.

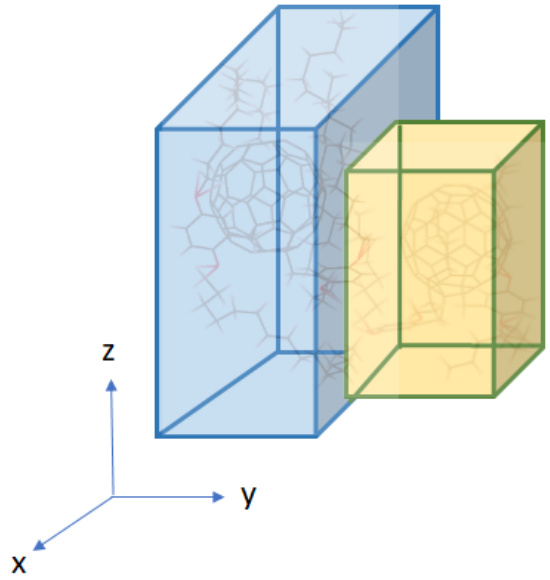

Figure 2. Theoretical DFT model of the disposition of HSS8 and HSS16 monomers in different orientations.

Table 2. Structural parameters, areas and volumes of C_{60}, PCBM, HSS8 and HSS16 monomers extracted by DFT calculations.

	Structural parameters [Å]			Area in different orientations [Å^2]			Volume [Å^3]
Materials	X	Y	Z	XY	YZ	XZ	XYZ
C_{60}	7.02	6.90	6.88	48.4	47.5	48.3	333.2

PCBM	14.79	9.82	6.96	145.2	68.4	102.9	1010.9
HSS8	12.24	15.58	16.62	190.7	258.9	203.4	3169.4
HSS16	18.52	19.18	20.82	355.2	399.3	385.6	7395.5

Complementary calculations were carried out under an implicit model of the solvent (Polarizable Continuum Model, PCM), making it possible to implicitly average the degrees of freedom of the solvent and to treat the electrostatic interactions (generally dominant in the solvation) for HS88 and HSS16 systems.[15] These new calculations show that neither the volumes nor the calculated surfaces are modified whatever the considered either chloroform or xylene.[15]

The results from chloroform effects reveal important information, i.e., that it is not the electrostatic interactions that govern the behavior of the HSS8 and HSS16 molecules in the solutions in our experiments as xylene and chloroform. The dielectric constant of chloroform and xylene is 4.809 and 2.562, respectively.[17] The origin of the observed differences between the PCM calculations and the experiments is, therefore, to be found elsewhere and in particular in the absence of explicit consideration of the first solvation layer in the PCM model. Because of its smaller size and the presence of chlorine, chloroform is, of the two solvents used in this work, the one that will most likely favor the setting up of these interactions by inserting itself more easily into the structures of the HSS8 and HSS16 molecules, automatically increasing the volume and the surfaces of these systems.[15]

2.2. Langmuir-Schaefer films

2.2.1. Atomic Force Microscopy

Figures 3 and 4 show the AFM images for the poly(fullerene) LS films fabricated from the materials solutions in chloroform and xylene, respectively. Table 3 summarizes the average roughness values obtained from these topographic images.

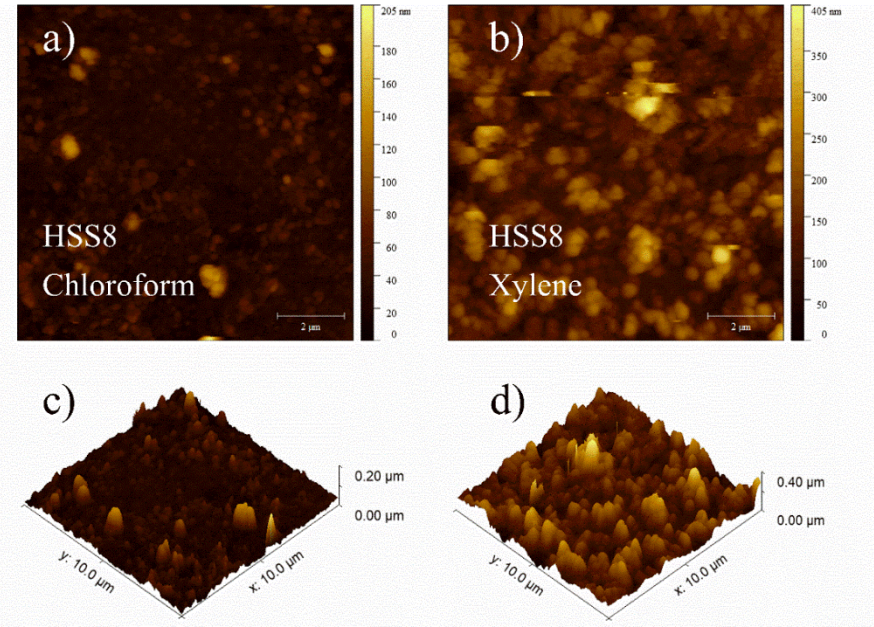

Figure 3. AFM images of HSS8 LS films obtained from chloroform (a and c) and xylene (c and d) solutions.

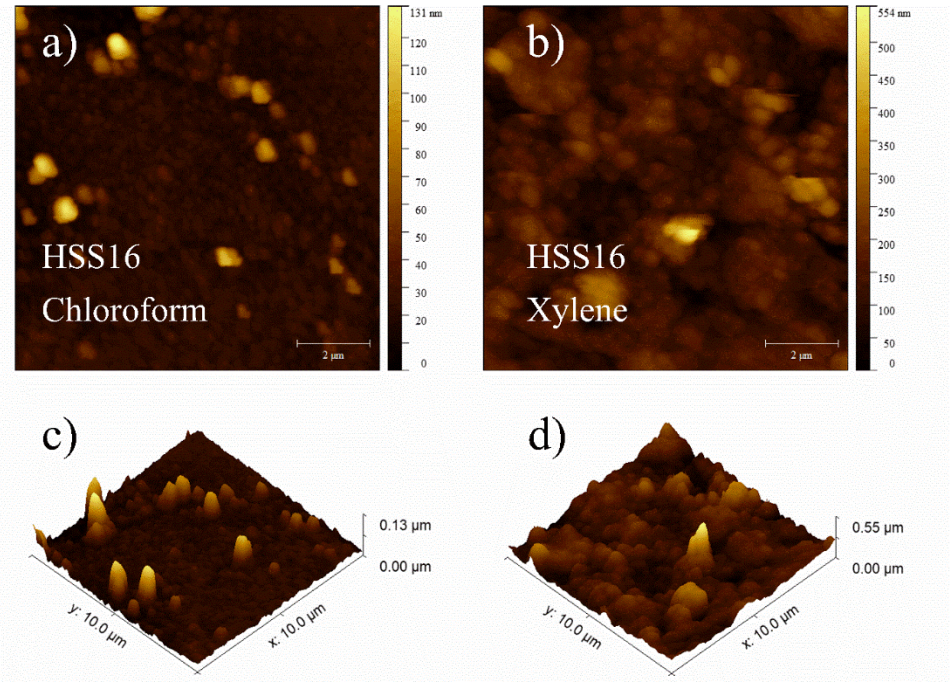

Figure 4. AFM images of HSS16 LS films obtained from chloroform (a and c) and xylene (c and d) solutions.

Table 3. Roughness values for poly(fullerene)s LS films.

Solvent	Root mean square roughness (nm)

	HSS8	HSS16
chloroform	15.6	12.6
xylene	49.5	57.0

According to the AFM results, the solvent used implies changes in the morphology of poly(fullerene)s, where for both films the root mean square (rms) roughness is lower and homogeneity is higher when using chloroform than xylene. Compared with chloroform, the rms roughness in xylene is 3.18 and 4.52 times higher in HSS8 and HSS16, respectively. This is associated with the solubility of the materials since it interferes with the organization of the molecules in the aqueous sub-phase of the Langmuir trough.

A relationship can be established between the roughness of LS films, the type of solvent used, and the mean molecular area of the Langmuir films. Significant differences are observed in the mean molecular area of Langmuir films when different solvents are utilized, specifically HSS8 with a 75% ↓(from chloroform to xylene) and HSS16 with a 73.8%↓ (from chloroform to xylene). These reductions indicate an increased formation of aggregates and packing in the Langmuir films when xylene is used as the solvent. During the transfer of Langmuir films to substrates, resulting in the formation of LS films, it appears that this aggregation is also transferred to the LS films, leading to rougher films when xylene is employed. Specifically, HSS8 68.48%↑ (from chloroform to xylene), and HSS16 77.8%↑ (from chloroform to xylene) in roughness. Furthermore, the properties of the solvent (xylene or chloroform) seem to be transferred as well. An inversely proportional relationship between the mean molecular area and the roughness of LS films can be inferred, showing a consistent pattern across the experimental conditions. As a result, LS films made with xylene as the solvent tend to have rougher surfaces compared to those made with chloroform.

2.2.2. Cyclic voltammetry, UV-Visible spectroscopy and DFT

Figures 5 to 6 show the third cycle in cyclic voltammograms for LS films of the HSS8 and HSS16 materials, solubilized in chloroform and xylene, on an ITO substrate, in a 0.1 mol/L solution of tetrabutylammonium perchlorate in acetonitrile, the sweeping was carried out at a scan rate of 50 mV/s. Whereas the HOMO and LUMO of materials are related to the ionization potential (by oxidation potential) and the electron affinity (by reduction potential), respectively.[18,19]

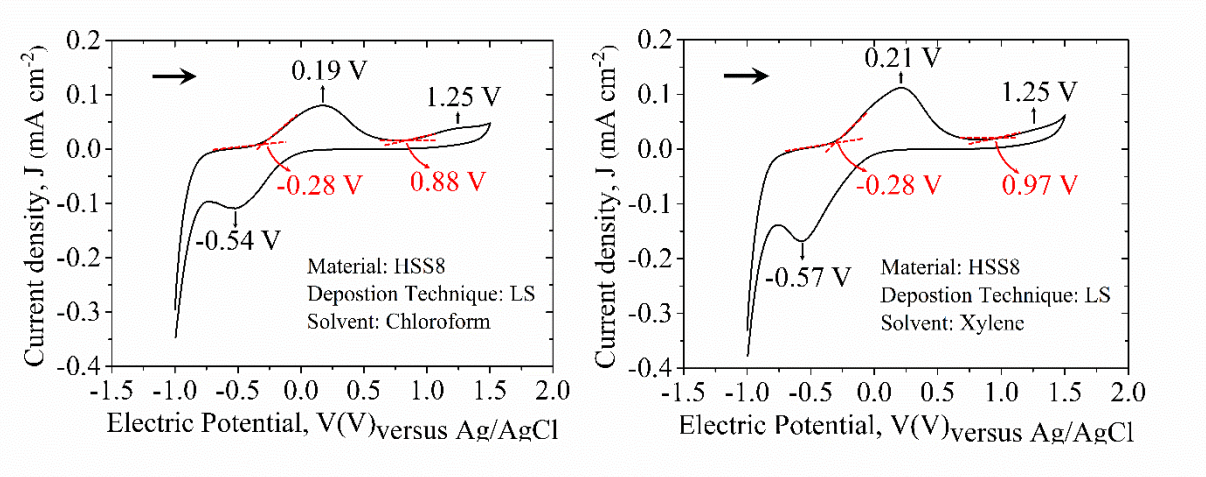

Figure 5. Cyclic voltammogram for LS films of HSS8 solubilized in chloroform (to the left) and xylene (to the right).

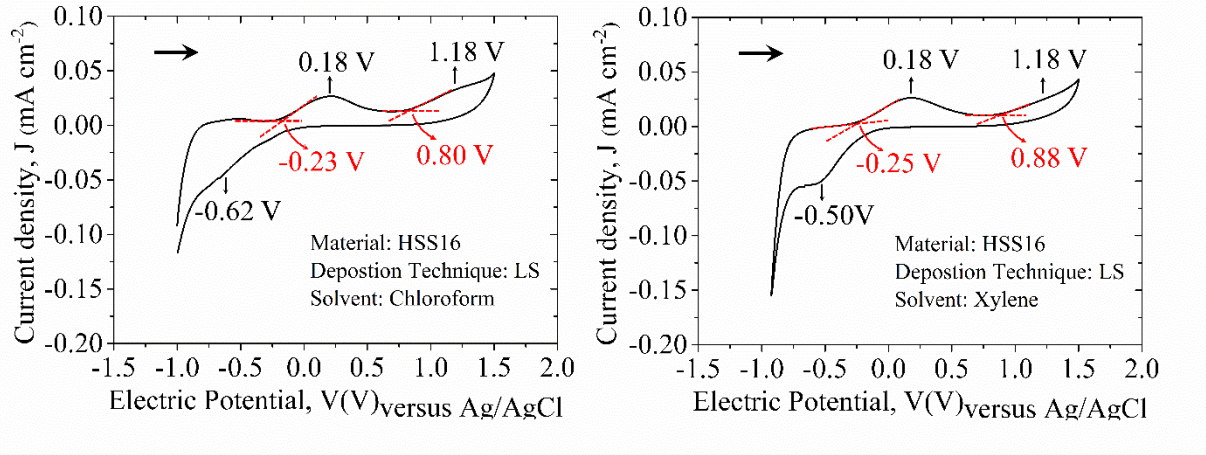

Figure 6. Cyclic voltammogram for LS films of HSS16 solubilized in chloroform (to the left) and xylene (to the right).

In the cyclic voltammograms shown in Figure 5, it is possible to observe that the LS film of HSS8 solubilized in chloroform has two oxidation peaks at 0.19 V and 1.25 V, and one reduction peak at -0.54 V, while the LS film solubilized in xylene shows the same pattern, with two reduction peaks at 0.21 and 1.25 V, and a reduction peak at -0.57 V. For the HSS16 films, in Figure 6 it is possible to observe that the LS film solubilized in chloroform has two oxidation peaks at 0.18 and 1.18 V, and one reduction peak at -0.62 V, while the LS film solubilized in xylene has two reduction peaks at 0.18 and 1.18 V, and one reduction peak at -0.50 V.

Since the measurements were carried out in solution and not under vacuum, the values must be corrected for each type of reference electrode and solution that was employed. The voltammograms show the ionization potential of the thin films at the point where the start of the current increase (onset) occurs before the first oxidation peak. The energy level for the

HOMO can be calculated through the relation $E_{HOMO} = -(E'_{OX} + 4.40)$, and for the Ag/AgCl/KCl electrode, the correction of 4.40 eV was considered.[20]

From the voltammograms, the E_{HOMO} calculated for the LS film of the HSS8, solubilized in chloroform and xylene, for is the same for both and equal to -4.23 eV, and for the second oxidation peak also the same for both and equal to -5.16 eV. This same pattern is observed for the first oxidation peak in the LS films of HSS8, where in both chloroform and xylene, the E_{HOMO} calculated for the first oxidation peak is- 4.12 eV, for the second oxidation peak is -5.28 and -5.37 eV in chloroform and xylene, respectively. For HSS16 LS films solubilized in chloroform, the E_{HOMO} calculated is -4.17 and -5.20 eV for the first and second oxidation peak, respectively, and in xylene is -4.15 and -5.28 eV for the first and second oxidation peak, respectively.

It was not possible to estimate the electronic affinity in the region of the cathodic potential of the voltammograms (related to the LUMO of the considered material) due to the difficulty to accurately determine the potentials' onset for the second reduction peak.[21] In spite of the electrochemical bandgap being usually higher than the optical bandgap in conjugated polymers, an outcome generally attributed to the formation of free ions in the electrochemical experiment rather than a neutral excited state. [21] So, the optical bandgap can be used in many cases as an approximation for electronic bandgaps, this was already reported for some low-bandgap polymers.

Thence, the optical bandgap energy (E_{gap}^{opt}) was obtained from the UV-Vis absorption measurements, the wavelength related to the optical bandgap is attained by the edge of the absorption spectrum of the film, and allows the calculation of the E_{gap}^{opt}.[22] The E_{gap}^{opt}can be calculated through the relation $E_{gap}^{opt} = \frac{hc}{\lambda} = \frac{1240}{\lambda} eV$, where h represents the Planck's constant in eV·s and c the speed of light in vacuum, in m/s.[22]

The absorption spectra of LS films show in chloroform (Figure 7) the absorption maximum at 356 and 368 nm for HSS8 and HSS16, respectively. In xylene (Figure 7) the same absorption maximum was shifted to 338 nm for both films. All LS films have a broad absorption maximum between 400 and 550 nm.

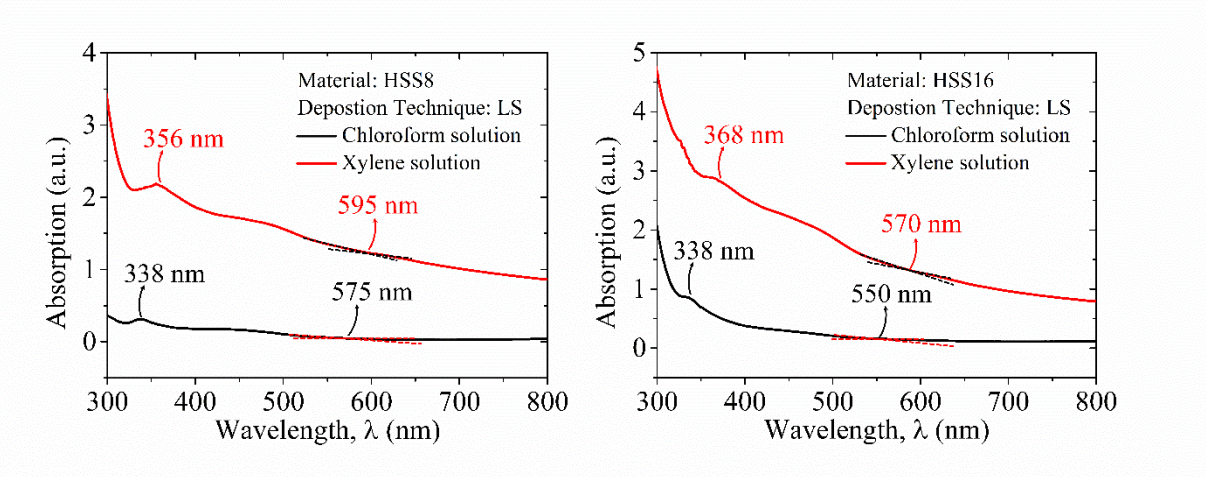

Figure 7. Absorption spectra for LS films of HSS8 (to the left) and HSS16 (to the right), both solubilized in chloroform or xylene.

Comparing with PCBM, in its spectrum has three feature peaks of fullerene derivatives, the [6-6]-addition at 260 nm, 330 nm (C_{60}) and 430 nm ([6,6]-addition in C_{60}).[12] In LS films, for both solvents, it is possible to observe the peak referring to C_{60}, and the broad absorption is an overlapping between the [6,6]-addition in C60 and 1,4-bis adducts (445 nm), that would result from the atom transfer radical addition polymerization (ATRAP) due to steric effects.[12] The broad absorption is also indicative of the presence of 1,2-adducts (400 nm).[12] The spectra show more peaks related to PCBM, and it is related to the large proportion of PCBM contained in the materials can overlapping many of the electronic properties of poly(fullerene)s.

The use of chloroform and xylene, as solvents, showed a difference in the position of the absorption peaks. This shows that the solvent influences not only the aggregation as shown in the study of isotherms, but also the absorption, in which he found that the propensity to form aggregates depends mainly on solvent polarization and has a direct relationship with the maximum absorption.

The E_{gap}^{opt} determined for the LS film of HSS8 solubilized in chloroform (λ_{onset} = 595 nm) was 2.10 eV and in xylene (λ_{onset} = 575 nm) was 2.15 eV. For HSS16, the LS film solubilized in chloroform (λ_{onset} = 570 nm) was 2.17 eV, and for film solubilized in xylene (λ_{onset} = 550 nm) was 2.25 eV. From the E_{HOMO} and E_{gap}^{opt} computed heretofore, it is conceivable to estimate the LUMO energy level, E_{LUMO}, by means of the relation $E_{LUMO} = E_{HOMO} + E_{gap}^{opt}$. Table 5 depicts the values aforementioned obtained for the films that will be used to estimate the energy diagrams. From the E_{gap}^{opt} values obtained, the materials can be classified as suitable for organic solar cells, as the most used materials reaching a band gap of up to 2.3 eV.[23]

Table 5. Values of E_{HOMO}, E_{LUMO} and E_{gap}^{opt} for polyfullerene LS films.

Thin film	Solvent	E_{HOMO}^{OXI} [eV]	E_{LUMO}^{OXI} [eV]	E_{HOMO}^{OXII} [eV]	E_{LUMO}^{OXII} [eV]	E_{gap}^{opt} [eV]
HSS8	chloroform	-4.12	-2.02	-5.28	-3.18	2.10
HSS8	xylene	-4.12	-1.97	-5.37	-3.22	2.15
HSS16	chloroform	-4.17	-1.97	-5.20	-3.03	2.17
HSS16	xylene	-4.15	-1.90	-5.28	-3.03	2.25

According to the DFT/6-31+G(d) results, for HSS8 monomer in vacuum, the E_{HOMO} E_{HOMO} is -5.36 eV, and the E_{LUMO} is -3.13 eV. Considering the chloroform effects, the E_{HOMO} and E_{LUMO} is -5.37 and -3.09 eV, respectively. In vacuum, for HSS16 monomer, the E_{HOMO} and E_{LUMO} is -5.36 and -3.18 eV, respectively, and in chloroform, the E_{HOMO} and E_{LUMO} is -5.35 and -3.13 eV, respectively. Comparing with experimental results, it is possible observe that the theoretical results are close to the experimental values calculated from the second oxidation peak, and the discrepancy between experimental values could be related to the CV measurements contains experimental errors and it is noticeable that solid-state packing effects are not included in the DFT calculations, which tend to affect the HOMO and LUMO energy levels in a thin film compared to an isolated monomer as considered in the calculations. [24,25,26]

3. Conclusion

Molecular organization in the solid state plays a central role on organic devices performance, from that this study has shown it is possible to successfully fabricate Langmuir and Langmuir-Schaefer films of short and long chain poly(fullerene) establishing a relation between structure and optoelectronics properties.

Through the π-A isotherms of poly(fullerene) Langmuir films, a strong indication of the formation of disordered aggregates in the aqueous subphase is shown, even when in good non-polar solvents, such as xylene, one cannot ignore the possibility that the PCBM readily form nanoaggregates. The use of different solvents changes the arrangement of molecules, indicating higher solubility and lower level of aggregation. From DFT calculations, to avoid 'crossing' each other, the arms of the HSS16 molecules (although surrounding mostly the fullerene) start

to extend, so the calculated molecular areas are all higher than the ones estimated in the π–A isotherms, indicating that both materials aggregate in the Langmuir trough.

The influence of solvent in LS films is also evidenced in AFM, UV-Vis and CV measurements. In AFM measurements the use of chloroform significantly reduced the roughness of poly(fullerene) LS films and presented a higher ordering compared to films prepared with xylene solutions. In UV-Vis measurements were found that the propensity to form aggregates depends mainly on the polarization of the solvent and is directly related to the maximum absorption and difference in the position of the absorption peaks. And in CV measurements, the type of solvent influences the oxidation and reduction peaks of the materials, consequently, in the HOMO and LUMO energy levels. From the optical bandgap energy values, the polyfullerenes studied here present high potential for application in organic electronic devices.

In the junction between DFT calculations and CV and UV-Vis measurements allowed the study of optoelectronic properties. The DFT/B3LYP/6-31+G(d) method provide LUMO values close to experimental values, thus being an important tool for comparing results, since there is no previous literature from these exact polyfullerenes.

4. Experimental Section/Methods

Poly(fullerene)s

Here was studied the opto-electronic and morphological properties of new classes of soluble main-chain poly(fullerene)s as shown in Figure 1. Namely, HSS8 (short sidechain) and HSS16 (long sidechains), were prepared as indicated in reference Santos Silva *et al*.[12] and all details on them can be found therein. The molecular weights of HSS8 were indicated to be: M_n = 920 g/mol, M_w = 1260 g/mol (dispersity, $Đ$ = 1.40) however, these values should be multiplied by at least five due to a mismatch between the polystyrene standards poly(fullerene)s, as indicated in that paper. Similarly, HSS16, has molecular weights indicated to be M_n = 3110 g/mol, M_w = 4610 g/mol while in reality are probably about five times higher. HSS16 $Đ$ = 1.48.

Fabrication and characterization of Langmuir films

The Langmuir films were prepared using a Langmuir trough KSV model 5000, being the aqueous subphase approximately 1350 mL of ultrapure water acquired from the Millipore water purification system, with a resistivity of 18.2 MΩ cm^{-1}. The solutions were prepared using HSS-8 (short sidechain) and HSS-16 (long sidechain) solubilized in chloroform or *ortho*-xylene at a concentration of 0.2 mg mL^{-1}. For obtaining the surface pressure per area per monomer, i.e.,

the π-A isotherm, the spread solutions onto the aqueous subphase at room temperature (23 ºC) and were compressed at 10 mm min^{-1} controlled by software.

Fabrication and characterization of Langmuir-Schaefer films

From stabilized Langmuir film, by a horizontal contact between the substrate and the monolayer while maintaining a constant surface pressure (SP), then slowly lifting the substrate, an LS film is made from one or more layers [27]. For the fabrication and characterization of the Langmuir-Schaefer (LS) films was used the same methodology in Langmuir films, where were deposited 15 layers onto indium-tin-oxide (ITO) substrates at a constant SP of 20 mN m^{-1} for morphological, electrochemical and optical measurements. ITO substrates were left over hexamethyldisilazane (HMDS) vapor in order to create a hydrophobic surface.

To obtain information on nanoscale morphology, atomic force microscopy (AFM) measurements were performed on the thin films (10 × 10 μm^2 area) using the Nanosurf EasyScan 2 Microscope with silicon probe coupled to a cantilever (Tap 190Al-G) and contact mode, where the operating mode was dynamic force with free vibration amplitude around 200 mV and vibration frequency of 155845 Hz. The number of measured data points per line was 512 and the time needed to acquire a data line was 1 s. The images obtained were treated and analyzed using the Gwyddion software (version 2.61).

The cyclic voltammetry measurements were carried out using an μAutolab Tipo III potentiostat/galvanostat, in a potential range of –1.5 to 1.5 V with a scan rate of 50 mV s^{-1}. This excitation cycle was repeated three times. The supporting electrolyte was a solution of 0.1 mol/L tetrabutylammonium perchlorate (TBAP) in acetonitrile (ACN). The cell was composed of an Ag/AgCl/KCl as the reference electrode, a platinum wire as the counter electrode and LS films over ITO substrates, with sheet resistance between 5 and 15 Ω, as the working electrode. UV-visible absorption spectroscopy measurements were performed in a Varian Cary 50 scan equipment, using the range from 300 nm to 900 nm.

Density Functional Theory

Since there is no previous literature from these exact polymers, to estimate monomer areas, were carried out the theoretical calculations using Density Functional Theory (DFT) with B3LYP exchange-correlation functional for optimizations of geometries and energies. All calculations were performed using the Gaussian 09 program package with, a relatively small and computationally cheap, 6-31G+(d) basis set. DFT calculations were combined with the

Grimme's D3 method to account for longer range dispersion interactions, and for solvation effects, the polarizable continuum model (PCM) was used in calculations.

Acknowledgements

The authors are grateful for the financial support of the Brazilian agencies São Paulo Research Foundation (FAPESP), INEO/CNPq (Instituto Nacional de Eletrônica Orgânica/ National Council for Scientific and Technological Development) and Coordenação de Aperfeiçoamento de Pessoal de Nível Superior (CAPES, nº 88882.330130/2019-01)

Received: ((will be filled in by the editorial staff))
Revised: ((will be filled in by the editorial staff))
Published online: ((will be filled in by the editorial staff))

References

[1] Z. Nasrollahi, M. Hashemi, S. Bameri, V. M. Taghvaee, *Environ. Dev. Sustain.* **2020**, *22*, 1105.

[2] N. V. Tran, Q. V. Tran, L. T. T. Do, L. H. Dinh, H. T. T. Do, *Energy*. **2019**, *173*, 483.

[3] H.-P. Wang, Jr-H. He, *Adv. Energy. Mater.* **2017**, *7*, 1602385.

[4] Y. Li, W. Huang, D. Zhao, L. Wang, Z. Jiao, Q. Huang, P. W. M. Sun, G. Yuan, *Molecules*. **2022**, *27*, 1800.

[5] N. Y. Doumon, L. YANG, F. Rosei, *Nano Energy*. **2022**, *94*, 106915.

[6] M. Günther, N. Kazerouni, D. Blätte, J. D. Perea, B. C. Thompson, T. Amer, *Nature Reviews Materials*, **2023**, 1.

[7] D. Zhou, J. Wang, Z. Xu, H. Xu, J. Quan, J. Deng, Y. Li, Y. Tong, B. Hu, L. Chen, *Nano Energy*. **2022**, 107802.

[8] K. Fukuda, K. Yu, T. Someya, *Adv. Energy. Mater.* **2020**, *10*, 2000765.

[9] G. Zhang, J. Zhao, P. C. Y. Chow, K. Jiang, J. Zhang, Z. Zhu, J. Zhang, F. Huang, H. Yan, *Chem. Rev.* **2018**, *118*, 3447.

[10] P. Meredith, W. Li, A. Armin. *Adv. Energy. Mater*. **2020**, *10*, 2001788.

[11] H. H. Ramanitra, H. S. Silva, B. A. Bregadiolli, A.l Khoukh, C. M. S. Combe, S. A. Dowland, D. Bégué, C. F. O. Graeff, C. Dagron-Lartigau, A. Distler, G. Morse, R. C. Hiorns, *Macromolecules*. **2016**, *49*, 1681.

[12] H. S. Silva, H. H. Ramanitra, B. A. Bregadiolli, D. Bégué, C. F. O. Graeff, C. Dagron-Lartigau, H. Peisert, T. Chassé, R. C. Hiorns, *J. Polym. Sci. A. Polym. Chem.* **2017**, *55*, 1345.

[13] O. N. Oliveira Jr, L. Caseli, K. Ariga, *Chem. Rev*. **2022**, *122*, 6459.

[14] L. V. L. Citolino, E. A. Silva, C. A. Olivati, *Mater. Sci. Semicond. Process*. **2019**, *91*, 296.

[15] W. D. Harkins, *The physical chemistry of surface films*, Reinhold Publishing Corp, NY, USA, **1952**.

[15] L. K. M. Roncaselli, E. A. Silva, M. L. Braunger, H. H. Ramanitra, M. Stephen, L. V. L. Citolino, J. D. Fernandes, A. V. S. Simõis, C. J. L. Constantino, D. L. Silva Agostini, D. Bégué, R. C. Hiorns, C. A. Olivati, *Phys. Chem. Chem. Phys.* **2022**, *24*, 12442.

[16] J. S. Peerless, G. H. Bowers, A. L.Kwansa, Y. G. Yingling, *J. Phys. Chem. B*. **2015**, *119*, 15344.

[16+1] E. A Silva, A. Gregori, J. D. Fernandes, C. Njel, R. Dedryvère, C. J. L. Constantino, R. C. Hiorns, C. Lartigau-Dagron, C. A. Olivati, *Nanotechnology*. **2020**, *31*, 315712.

[17] R. S. Ruoff, D. S. Tse, R. Malhotra, D. C. Lorents, *J. Phys. Chem.* **1993**, *97*, 3379.

[18] L. Leonat, G. Sbarcea, I. V. Branzoi., *UPB Sci. Bull. Ser. B.* **2013**, *75*, 111.

[19] J. Sworakowski., *Synth. Met.* **2018**, *235*, 125.

[20] L. Micaroni, F. Nart, I. Hümmelgen, *J. Solid State Electrochem.*, **2002**, *7*, 55.

[21] D. Baran, A. Balan, S. Celebi, B. M. Esteban, H. Neugebauer, N. S. Sariciftci, L. Toppare, *Chem. Mater*. **2010**, 22, 2978.

[22] M. L. Braunger, A. Barros, M. Ferreira, C. A. Olivati, *Electrochim Acta*. **2015**, *165*, 1.

[23] Y. Wang, D. Qian, Y. Cui, H. Zhang, J. Hou, K. Vandewal, T. Kirchartz, F. Gao, *Adv. Energy. Mater.* **2018**, *8*, 1801352.

[24] J. L. Brédas, J. P. Calbert, D. A. da Silva Filho, J. Cornil. *PNAS. 2002*, *99*, 5804.

[25] H. Bronstein, C. B. Nielsen, B. C. Schroeder, I. McCulloch, *Nat. Rev. Chem*. **2020**, *4*, 66.

[26] M. Pasinia, B. Vercellib, G. Zottic, A. Berlind, *Electrochim. Acta*. **2016**, *193*, 261.

[27] L. V. L. Citolino, M. L. Braunger, V. J. R. Oliveira, C. A. Olivati, *Mater. Res.* **2017**, 20, p. 874.